15th World Congress on Computational Mechanics (WCCM-XV)
8th Asian Pacific Congress on Computational Mechanics (APCOM-VIII)
Virtual Congress: 31 July – 5 August 2022
S. Koshizuka (Ed.)

PRACTICAL BOUNDARY CONDITIONS FOR ELECTRONIC STRUCTURE CALCULATIONS

EIJI TSUCHIDA[1]

[1] National Institute of Advanced Industrial Science and Technology (AIST), Tsukuba Central 2,
Umezono 1-1-1, Tsukuba 305-8568, Japan
Eiji.Tsuchida@aist.go.jp

Key words: molecular dynamics; density-functional theory; symmetry; gamma point; boundary conditions

Abstract. *Computational materials design is an active area of research which aims at predicting physical and chemical properties of various materials from first-principles electronic structure calculations. To keep the computational costs manageable, the Schrödinger equations are often approximated by Kohn-Sham equations within the framework of density-functional theory. These Kohn-Sham equations are solved numerically either by a basis set expansion or real-space discretization under given boundary conditions. In the case of a plane-wave basis set, it is common practice to apply periodic boundary conditions in all directions, while isolated boundary conditions are more common for the atomic basis set. However, there are many other options besides these standard boundary conditions. In this presentation, we will explore several non-standard boundary conditions which exploit the characteristics of each system, such as surfaces, interfaces, and cyclic/helical structures, to minimize the computational costs of electronic structure calculations. Most of these boundary conditions are easily implemented by minor modifications of existing electronic structure codes. Numerical examples on a few model systems are also presented for the validation of these boundary conditions.*

1 INTRODUCTION

In standard band-structure calculations within the framework of density-functional theory, the electron orbitals are obtained from the Kohn-Sham equations [1]. These equations are solved numerically either by a basis set expansion or real-space discretization under the periodic boundary conditions (PBCs). The unit cell typically contains ≤ 100 atoms, and symmetry of the atomic configuration is exploited to minimize the number of k-points required for Brillouin zone sampling [2]. In recent years, however, it has become routine to use a large supercell containing hundreds of atoms in conjunction with Γ-point sampling of the Brillouin zone. At variance with the electron orbitals sampled at the general k-points, the Γ-point orbitals are real-valued, and have full symmetry of the system. Some of the standard plane-wave codes are equipped with a special version which exploits the former property, but the latter is often neglected. Nevertheless, the use of symmetry is an attractive option even for the Γ-point sampling, leading to a dramatic reduction of computational costs for static calculations of perfect crystals. Examples of such applications include molecular crystals, intermetallic compounds, clathrate hydrates, and porous materials (metal-organic frameworks, covalent-organic frameworks, and zeolites), some of which are shown in Fig.1(a)-(b). Besides the ground-state calculations, the use of symmetry can also accelerate the evaluation of the Hessian matrix [3] and excited spectra [4]. This approach is a well-established technique for the atomic basis set [5, 6], making possible *ab initio* calculations of large systems which

are otherwise intractable. In contrast, it is a challenging task to exploit all possible symmetry operations in a systematic basis set like plane-waves and real-space grids for the following reasons [7, 8]:
(i) In the case of real-space methods, the computational domain differs for each symmetry operation, which has a negative impact on the performance on a parallel computer. Similarly, for plane-waves, it is not an easy task to prepare a fully optimized fast Fourier transform (FFT) library which is compatible with any combination of symmetry operations.
(ii) When crystalline symmetry is taken into account, the Hamiltonian becomes a block-diagonal matrix, with each block corresponding to a different symmetry group [5, 9]. However, the number of occupied states for each symmetry group is usually not known in advance [7, 9]. This uncertainty complicates the iterative diagonalization of the Hamiltonian significantly.
(iii) In principle, the ground-state electron density obtained from symmetry-unrestricted calculations may have lower symmetry than that of the atomic configuration. This *symmetry breaking* is known to occur often in a system containing open-shell atoms [10, 11], but the correct symmetry is not always predictable. A possible solution is to perform the stability analysis via the electronic Hessian [12, 13]. At present, it is not clear whether the computational cost of this procedure for a systematic basis set is acceptable or not.

Moreover, for condensed matter systems at finite temperature, the atoms move irregularly and often diffuse in time, and thus any symmetry inherent in the initial configuration is lost. Nevertheless, it is often possible to benefit from the use of symmetry which reflects the characteristics of each system. In what follows, we will illustrate several non-standard boundary conditions which are effective for modeling real-world problems.

Let us consider simulating a two-phase system using a supercell that is as small as possible. One possible choice is to impose either the inversion symmetry, or mirror-reflection symmetry in a direction perpendicular to the interface. These symmetry operations lead to multiple fixed points in the cell, which may be acceptable for fixed bulk layers compatible with these symmetry operations. In the liquid phase, however, the atomic motion suffers from artifacts due to the strong interactions between an atom and its image near these fixed points [14]. A better solution to this problem is to apply the glide-reflection symmetry which consists of mirror reflection in one direction, followed by a translation in the perpendicular direction. At variance with the inversion/mirror-reflection symmetry, the glide-reflection symmetry has no fixed points in the cell, and thus allows us to model a wide range of two-phase systems effectively, such as solid-liquid interfaces (Fig.1(c)), using only half of the cell explicitly. The validity of this method is demonstrated in previous studies within the classical simulations [14, 15, 16, 17, 18], with a significant reduction of computational time. The glide-reflection symmetry is also promising for nonequilibrium simulations of liquids and soft materials which use two reservoirs to generate a gradient of temperature, velocity, and density in the unit cell. These simulations aim at calculating transport properties, such as viscosity and thermal conductivity (Fig.1(d)) [19].

Cyclic and helical symmetry operations form another class of important symmetry groups, and are characteristic of many technologically important systems, such as nanotubes, collagen, synthetic helical polymers, and liquid crystals. These symmetry operations are usually implemented assuming periodicity in the axial direction, while isolated boundary conditions are applied in the radial direction. This approach allows us to perform electronic structure calculations of nanostructures possessing very long periods ($>$ 100 Å) at reasonable computational costs [20]. On the other hand, the use of isolated boundary conditions is not appropriate when these nanostructures are surrounded by explicit solvent molecules, particularly at finite temperature. Here we consider the use of cyclic/helical symmetry in conjunction

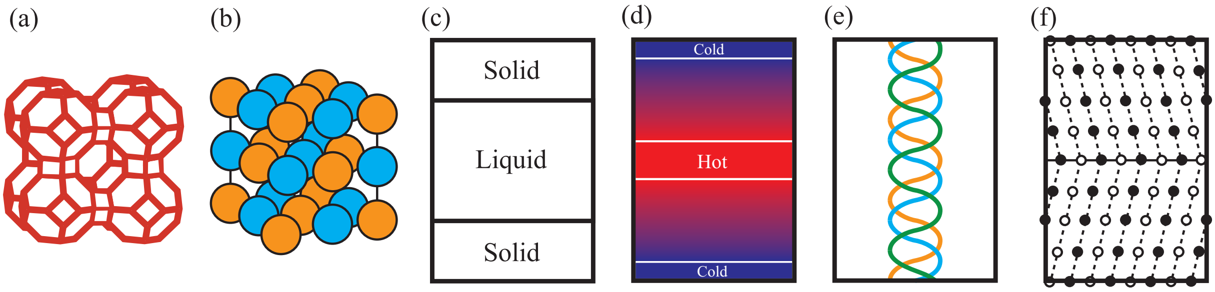

Figure 1: Potential applications of various symmetry operations compatible with PBCs: (a) LTA zeolite, (b) molecular crystal, where the orange and blue spheres represent C_{60} and a transition metal complex, respectively, (c) solid-liquid interfaces, (d) nonequilibrium molecular dynamics of liquids using two thermostats [24], (e) collagen forming a triple-helix structure, and (f) grain boundaries [25].

with PBCs in all directions. Under these circumstances, the rotational angles are limited to multiples of $\pi/3$ or $\pi/2$ [21, 22, 23], where a hexagonal lattice is required for the former, and a tetragonal lattice for the latter.

It is important to note that the cyclic PBC mentioned above is associated with multiple fixed points, such as the edge of the cell as well as the center of rotation, leading to severe restrictions on the atomic motion near these points. In contrast, the helical PBC does not suffer from such artifacts due to the absence of fixed points. A special case of the helical PBC, hereafter referred to as anti-periodic boundary conditions [25], consists of a π rotation, followed by a translation in the axial direction. This method is well suited for the modeling of diverse systems possessing $P2_1$ symmetry, as illustrated in Fig.1(e),(f). At variance with the glide-reflection boundary conditions, the anti-periodic boundary conditions retain the chirality of the molecules [15], and thus are more appropriate for modeling molecular systems of biological interest, such as lipid bilayers.

2 THEORY

Let us assume that PBCs are applied in all directions using an orthorhombic supercell of size $L_x \times L_y \times L_z$, hereafter referred to as the parent cell. Then, the Hamiltonian H will satisfy

$$H(x+n_xL_x, y+n_yL_y, z+n_zL_z) = H(x,y,z) \tag{1}$$

for any set of integers (n_x, n_y, n_z). Assuming Γ-point sampling of the Brillouin zone, the electron orbital also satisfies

$$\psi(x+n_xL_x, y+n_yL_y, z+n_zL_z) = \psi(x,y,z). \tag{2}$$

Now we discuss the implementation of a few additional boundary conditions which are compatible with the parent cell.

The glide-reflection boundary conditions mentioned in Sec.1 can be written as

$$H(x \pm L_x/2, y \pm L_y/2, L_z - z) = H(x,y,z), \tag{3}$$

where the signs are used for wrapping the coordinates. This operation consists of mirror reflection with respect to the glide-plane $z = L_z/2$, followed by a translation of $(L_x/2, L_y/2, 0)$. The corresponding eigenfunction satisfies

$$\psi(x \pm L_x/2, y \pm L_y/2, L_z - z) = \pm\psi(x,y,z). \tag{4}$$

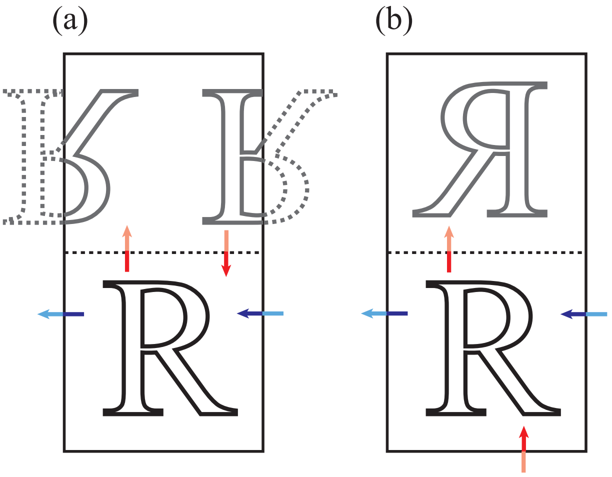

Figure 2: (a) Glide-reflection and (b) anti-periodic boundary conditions in 2D. The arrows indicate how the coordinates are wrapped in each direction.

This procedure ensures that the parent cell has no net dipole in the z-direction, thus eliminating the need for dipole corrections.

Similarly, the anti-periodic boundary condition is given by

$$H(L_x - x, L_y - y, z \pm L_z/2) = H(x,y,z), \tag{5}$$

which consists of a π rotation with respect to the z-axis, followed by a translation of $L_z/2$ along the z-axis. The corresponding eigenfunction satisfies

$$\psi(L_x - x, L_y - y, z \pm L_z/2) = \pm\psi(x,y,z), \tag{6}$$

and thus the x- and y-components of the dipole moment cancels out.

In what follows, we show how to implement these boundary conditions in electronic structure calculations. In the case of a plane-wave basis set, $\psi(\mathbf{r})$ is given by an expansion of the form

$$\psi(\mathbf{r}) = \frac{1}{\sqrt{V_{\text{cell}}}} \sum_{\mathbf{G}} c(\mathbf{G}) \cdot \exp(i\mathbf{G}\cdot\mathbf{r}), \tag{7}$$

where $\mathbf{G}$ is a reciprocal vector of the parent cell defined by $\mathbf{G} = 2\pi(n_x/L_x, n_y/L_y, n_z/L_z)$, and the sum runs over all $\mathbf{G}$'s which satisfy $|\mathbf{G}|^2 \le E_{\text{cut}}$, the cutoff energy. Thanks to the translational invariance of plane waves, Eq.(2) is automatically satisfied for any $\mathbf{r}$. Since the elecron orbitals sampled at the Γ-point are real, i.e., $\psi^*(\mathbf{r}) = \psi(\mathbf{r})$,

$$c^*(\mathbf{G}) = c(-\mathbf{G}) \tag{8}$$

holds for any $\mathbf{G}$ [26]. Therefore, only half of the total coefficients need to be stored explicitly. Further reduction of the coefficients is possible through the use of symmetry, as follows. In the case of glide-reflection boundary conditions, the following relation holds:

$$c(\mathbf{G}) = c(G_x, G_y, G_z) = \pm c(G_x, G_y, -G_z) \times (-1)^{n_x+n_y}, \tag{9}$$

which is derived from Eqs.(4) and (7). Similarly, for the anti-periodic case,

$$c(\mathbf{G}) = \pm c(-G_x, -G_y, G_z) \times (-1)^{n_z} \tag{10}$$

is derived from Eqs.(6) and (7). These simple relations allow us to reduce the number of variables by another factor of two.

One of the most time-consuming steps in plane-wave calculations is the Fourier transformation between real and reciprocal space. Many plane-wave codes rely on external FFT libraries which are highly optimized for 3D real-valued data, often including extensions to GPU. As mentioned in Sec.1, it is not an easy task to make these libraries compatible with any combination of symmetry operations without a loss of efficiency. If, however, only one of the conditions, either Eq.(9) or (10), needs to be taken into account, optimized FFT libraries can be developed with modest effort.

On the other hand, in the case of real-space discretization such as the finite-difference and finite-element methods [27, 28, 29, 30, 31, 32], the electron orbitals are represented by their values on a discrete grid, and thus Eqs.(2), (4), and (6) are immediately realized by using only half of the parent cell. Then, the number of variables is reduced by a factor of two in a straightforward manner. When the lower half of the parent cell is used as the computational domain, the coordinates are wrapped as indicated by the arrows in Fig.2. The interprocessor communications are slightly affected by the change from ordinary PBCs, but there is practically no overhead.

A few remarks common to both methods are given below:
(i) When symmetry is taken into account, some variables, such as $c(\mathbf{G}=0)$, contribute to the total energy with higher/lower multiplicities. This bias may lead to slow convergence during the iterative diagonalization of the Hamiltonian, and thus should be removed by rescaling the variables appropriately.
(ii) The numerical grid, which is used to evaluate the electron density, must be compatible with the symmetry of the atomic configuration [27]. Violation of this restriction leads to undesirable symmetry degradation.
(iii) For computationally inexpensive procedures which spend only a small portion of the total time, the use of the whole parent cell, which is somewhat redundant, is acceptable to minimize human efforts.

3 RESULTS

To demonstrate the effectiveness of boundary conditions illustrated in Sec.2, we calculate the eigenvalues of the Schrödinger equation,

$$\left(-\nabla^2 + V(\mathbf{r})\right)\psi(\mathbf{r}) = \lambda\psi(\mathbf{r}), \tag{11}$$

in two 2D model systems. Here the potential function is given by

$$V(\mathbf{r}) = \sum_{\mathbf{L}} \sum_{i=1}^{N_{\mathrm{atom}}} v(|\mathbf{r} - \mathbf{R}_i + \mathbf{L}|), \tag{12}$$

where $\mathbf{R}_i$ denotes the position of the i-th (pseudo)atom in the primary cell, $\mathbf{L}$ the lattice vector, and $v(r) = v_0 \cdot \exp(-r^2/r_c^2)$ with $v_0 = -32$ and $r_c = 0.5$. The Hamiltonian matrix was diagonalized using DSYEV, the dense matrix routine of the LAPACK library. Assuming a single bound state per atom, the ground-state energy for each model is defined by $E_G = \sum_{i=1}^{N_{\mathrm{atom}}} \varepsilon_i$, where ε_i denotes the i-th lowest eigenvalue.

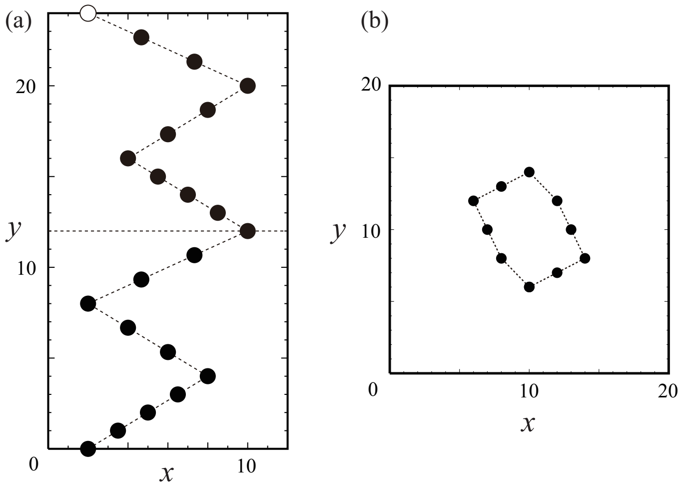

Figure 3: Atomic configuration of the 2D model systems used in this work: the first model (a) satisfies $(x', y') = (L_x - x, y \pm L_y/2)$, while the second model (b) is characterized by $(x', y') = (L_x - x, L_y - y)$.

The first model consists of 20 atoms in a rectangular supercell of $L_x = 12, L_y = 24$. The atomic configuration was chosen to satisfy the anti-periodic boundary conditions along the y-axis, or equivalently, the glide-reflection symmetry with respect to the glide-plane of $x = L_x/2$, as shown in Fig.3(a). The eigenvalues and the ground-state energies for this model were calculated using a plane-wave basis set as well as the higher-order finite-difference method [33]. The results shown in Table 1 indicate that both methods give the same results up to near machine precision, and the eigenvalues obtained from symmetry-unrestricted calculations for the whole cell consist of 10 pairs of nearly degenerate eigenvalues, reflecting the large distances between symmetrically equivalent atoms. We have also calculated the eigenvalues for the same model assuming $\psi(x', y') = \psi(x, y)$ using the plane-wave basis set. The 10 eigenvalues obtained from these symmetry-restricted calculations are found to reproduce one of each pair obtained from the symmetry-unrestricted calculations. The remaining eigenvalues may also be obtained by performing symmetry-restricted calculations under $\psi(x', y') = -\psi(x, y)$. However, considering the small splitting of the eigenvalues and perfect agreement of E_G, this procedure can be omitted without any loss of accuracy. Assuming that the computational cost of matrix diagonalization scales cubically with system size, the results of symmetry-unrestricted calculations can be obtained at only 1/8 of the original cost by exploiting symmetry.

The second model is described by 10 atoms in a square supercell of $L_x = L_y = 20$. The atomic configuration has 2-fold rotational symmetry, or equivalently, the inversion symmetry with respect to the center of the cell, as shown in Fig.3(b). For this model, we focused on the plane-wave basis set. The eigenvalues for this system are found to consist of five close pairs, as shown in Table 2. At variance with the first model, the splitting of the eigenvalues is found to be non-negligible due to the short distances between symmetrically equivalent atoms. Therefore, we have performed symmetry-restricted calculations for symmetric and anti-symmetric orbitals separately. When both conditions were taken into account, we were able to reproduce all eigenvalues of the symmetry-unrestricted calculations at $2/8 = 1/4$ of the original cost. Moreover, the ground-state energies obtained from symmetry-restricted calculations are found to show much better agreement than the individual eigenvalues, suggesting that either one of the

Table 1: Ground-state energies and eigenvalues for the first model, obtained from symmetry-unrestricted and restricted calculations. E_G is multiplied by 2 in the latter case. FD and PW denote the finite-difference method (near convergence) and plane-waves (at full convergence), respectively.

	Unrestricted (FD)	Unrestricted (PW)	Restricted (PW, +)
$E_G(\times 2)$	-271.131139448870	-271.131139447908	-271.131139447924
Eigenvalues			
1	-13.7340214731321	-13.7340214730857	-13.7340214730813
2	-13.7340214715735	-13.7340214715261	
3	-13.6632209260106	-13.6632209259640	
4	-13.6632209112884	-13.6632209112425	-13.6632209112406
5	-13.5669633670584	-13.5669633670075	-13.5669633670164
6	-13.5669554071918	-13.5669554071424	
7	-13.5617884878583	-13.5617884878114	
8	-13.5617729183291	-13.5617729182823	-13.5617729182890
9	-13.5508727426596	-13.5508727426093	-13.5508727426044
10	-13.5508323265460	-13.5508323264995	
11	-13.5490604512204	-13.5490604511712	
12	-13.5489973210613	-13.5489973210131	-13.5489973210105
13	-13.5483766628785	-13.5483766628339	-13.5483766628347
14	-13.5483460125231	-13.5483460124770	
15	-13.5361127271807	-13.5361127271308	
16	-13.5361124132121	-13.5361124131643	-13.5361124131604
17	-13.4642552251408	-13.4642552250898	
18	-13.4642552249509	-13.4642552249021	-13.4642552249028
19	-13.3909766898669	-13.3909766898158	-13.3909766898214
20	-13.3909766891877	-13.3909766891389	

symmetry-restricted calculations may be sufficient. At present, however, it remains unclear whether this holds true in more realistic problems as well.

4 DISCUSSIONS

So far, we have considered only orthogonal cells. However, nonorthogonal cells are often desirable for efficient simulations of diverse problems. For instance, body centered cubic (BCC) and face centered cubic (FCC) lattices are very useful for modeling defects in solids [34, 35], solvated macromolecules [36, 37, 38], and homogeneously disordered systems [39, 40]. The hexagonal close-packed (HCP) lattice (or more generally, the hexagonal prism) can minimize the number of explicit solvent molecules in the cell when simulating linear/helical molecules in solution, such as DNA and collagen [41, 42].

It is straightforward to use these lattices in a standard plane-wave code. In contrast, a naïve implementation of these lattices in a real-space code introduces a significant loss of efficiency when calculating the kinetic energy of electrons [43, 44, 45]. This problem may be overcome by using the sliding-brick representation of these lattices. In this representation, the unit cell is kept orthogonal, while each cell is arranged alternately [46, 47, 48, 49] (Fig.4). This method allows us to use orthogonal grids within each cell, and can be viewed as a special case of the Lees-Edwards boundary conditions which are used

Table 2: Ground-state energies and eigenvalues for the second model, obtained from symmetry-unrestricted and restricted plane-wave calculations at full convergence. E_G is multiplied by 2 in the latter case.

	Unrestricted	Restricted (+)	Restricted (-)
$E_G(\times 2)$	-135.504345023854	-135.5043451175664	-135.5043449301426
Eigenvalues			
1	-13.5822869068064	-13.5822869068048	
2	-13.5816976666550		-13.5816976666543
3	-13.5692019924984		-13.5692019925012
4	-13.5673772957633	-13.5673772957634	
5	-13.5517001228019	-13.5517001228023	
6	-13.5492737234649		-13.5492737234671
7	-13.5329855223182		-13.5329855223186
8	-13.5311675409852	-13.5311675409850	
9	-13.5196406924283	-13.5196406924277	
10	-13.5190135601320		-13.5190135601301

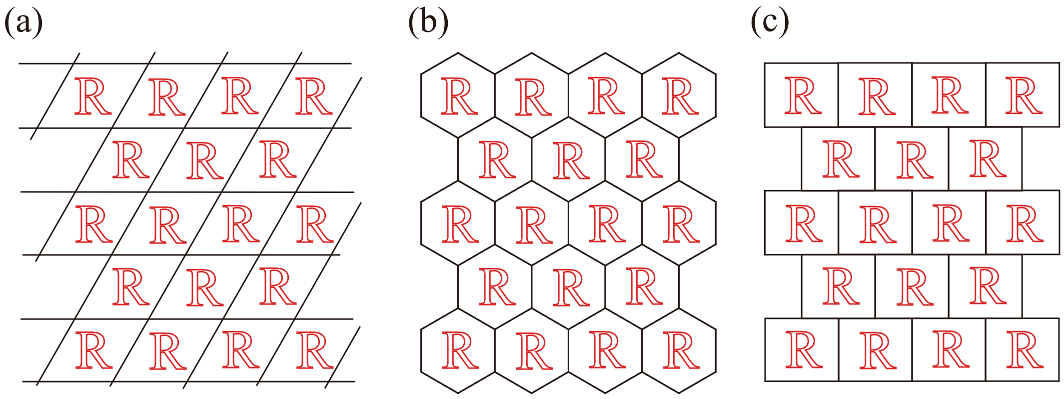

Figure 4: Three different but equivalent forms of a 2D hexagonal lattice : (a) Bravais lattice, (b) Wigner-Seitz cell, and (c) sliding-brick representation.

in a wide range of nonequilibrium simulations [39, 50]. This representation is particularly effective for BCC/FCC lattices whose unit cells have simple integer ratios in all directions, as shown in Table 3. On the other hand, this approach is less favorable for the HCP lattice, because the unit cell has a non-integer ratio, which is undesirable for real-space discretization. An alternative solution is to apply the discretization formula of the Laplacian developed for the hexagonal lattice (Fig.4 (b)) [43, 44] which retains 6-fold rotational symmetry.

5 CONCLUSIONS

In this work, we have presented several non-standard boundary conditions which can minimize the computational cost of *ab initio* molecular dynamics simulations in many technologically important systems, such as solid-liquid interfaces and hydrated biomolecules. These boundary conditions are also promising for nonequilibrium simulations of liquids and soft materials targeting transport properties,

Table 3: Definition of orthogonal unit cells in the sliding-brick representation of BCC, FCC, and HCP lattices. Translation vectors are equal to those of the underlying Bravais lattices.

Lattice	Cell size	V_{cell}
BCC	$a \times a \times \frac{1}{2}a$	$\frac{1}{2}a^3$
FCC	$\frac{1}{2}a \times \frac{1}{2}a \times a$	$\frac{1}{4}a^3$
HCP	$2a \times \sqrt{3}a \times c$	$2\sqrt{3}a^2c$

such as viscosity and thermal conductivity. Implementation of these boundary conditions in existing electronic structure codes is straightforward for both real-space and plane-wave basis sets under PBCs.

ACKNOWLEDGMENTS

Part of the calculations were carried out using the computer facilities at Research Institute for Information Technology, Kyushu University. This work was supported by JST CREST Grant Number JPMJCR18I4, Japan.

REFERENCES

[1] Martin, R. M., *Electronic Structure: Basic Theory and Practical Methods*, Cambridge University Press, New York, 2004.

[2] Kratzer, P. and Neugebauer, J., *Front. Chem.* (2019) **7**: 106.

[3] Gan, C.K., Liu, Y., Sum, T.C., and Hippalgaonkar, K., Efficacious symmetry-adapted atomic displacement method for lattice dynamical studies, *Comput. Phys. Commun.* (2021) **259**: 107635.

[4] Gao, W. and Chelikowsky, J.R., Accelerating Time-Dependent Density Functional Theory and GW Calculations for Molecules and Nanoclusters with Symmetry Adapted Interpolative Separable Density Fitting, *J. Chem. Theory Comput.* (2020) **16**: 2216-2223.

[5] Erba, A., Baima, J., Bush, I., Orlando, R., and Dovesi, R., Large-Scale Condensed Matter DFT Simulations: Performance and Capabilities of the CRYSTAL Code, *J. Chem. Theory Comput.* (2017) **13**: 5019-5027.

[6] Rusakov, A.A., Frisch, M.J., and Scuseria, G.E., Space group symmetry applied to SCF calculations with periodic boundary conditions and Gaussian orbitals, *J. Chem. Phys.* (2013) **139**: 114110.

[7] Fang, J., Gao, X., and Zhou, A., A Symmetry-Based Decomposition Approach to Eigenvalue Problems, *J. Sci. Comput.* (2013) **57**: 638-669.

[8] Schlosser, H., Symmetrized combinations of plane waves and matrix elements of the hamiltonian for cubic lattices, *J. Phys. Chem. Solids* (1962) **23**: 963-969.

[9] Young, D.C., *Computational Chemistry*, Wiley-Interscience, 2001.

[10] Cramer, C.J. and Truhlar, D.G., Density functional theory for transition metals and transition metal chemistry, *Phys. Chem. Chem. Phys.* (2009) **11**: 10757-10816.

[11] Chowdhury, S.T. ur R. and Perdew, J.P., Spherical vs non-spherical and symmetry-preserving vs symmetry-breaking densities of open-shell atoms in density functional theory, *J. Chem. Phys.* (2021) **155**: 234110.

[12] Bauernschmitt, R. and Ahlrichs, R., Stability analysis for solutions of the closed shell Kohn-Sham equation, *J. Chem. Phys.* (1996) **104**: 9047-9052.

[13] Sharada, S.M., Stück, D., Sundstrom, E.J., Bell, A.T., and Head-Gordon, M., Wavefunction stability analysis without analytical electronic Hessians: application to orbital-optimised second-order Møller-Plesset theory and VV10-containing density functionals, *Mol. Phys.* (2015) **113**: 1802-1808.

[14] Wong, K-Y. and Pettitt, B.M., A new boundary condition for computer simulations of interfacial systems, *Chem. Phys. Lett.* (2000) **326**: 193-198.

[15] Dolan, E.A., Venable, R.M., Pastor, R.W., and Brooks, B.R., Simulations of Membranes and Other Interfacial Systems Using $P2_1$ and P_c Periodic Boundary Conditions, *Biophys. J.* (2002) **82**: 2317-2325.

[16] Prasad, S., Simmonett, A.C., Meana-Pañeda, R., and Brooks, B.R., The Extended Eighth-Shell method for periodic boundary conditions with rotational symmetry, *J. Comput. Chem.* (2021) **42**: 1373-1383.

[17] Van den Branden, G., Baelmans, M., and D'haeseleer, W., The shifted reflective boundary for the study of two-phase systems with molecular dynamics simulations, *Mol. Phys.* (2008) **106**: 43-56.

[18] Wong, K.-Y. and Pettitt, B.M., Orientation of DNA on a surface from simulation, *Biopolymers* (2004) **73**: 570-578.

[19] Müller-Plathe, F., *J. Chem. Phys.* (1997) **106**: 6082-6085.

[20] Banerjee, A.S. and Suryanarayana, P., Cyclic density functional theory: A route to the first principles simulation of bending in nanostructures, *J. Mech. Phys. Solids* (2016) **96**: 605-631.

[21] Frenkel, D., Simulations: The dark side, *Eur. Phys. J. Plus* (2013) **128**: 10.

[22] Allen, M.P. and Masters, A.J., Computer simulation of a twisted nematic liquid crystal, *Mol. Phys.* (1993) **79**: 277-289.

[23] Kessler, J. and Bouř, P., Molecular dynamics with helical periodic boundary conditions, *J. Comput. Chem.* (2014) **35**: 1552-1559.

[24] Tsuchida, E., Thermal Conductivity of Liquid Water from Reverse Nonequilibrium Ab Initio Molecular Dynamics, *J. Phys. Soc. Jpn.* (2018) **87**: 025001.

[25] Hardouin Duparc, O.B.M. and Torrent, M., A new type of periodic boundary condition useful for high-temperature atomistic simulations of grain boundaries: Applications in semiconductors, *Interface Sci.* (1994) **2**: 7-16.

[26] Marx, D. and Hutter, J., *Ab Initio Molecular Dynamics: Basic Theory and Advanced Methods*, Cambridge University Press, Cambridge, 2009.

[27] Kronik, L., Makmal, A., Tiago, M.L., Alemany, M.M.G., Jain, M., Huang, X., Saad, Y., and Chelikowsky, J.R., PARSEC - the pseudopotential algorithm for real-space electronic structure calculations: recent advances and novel applications to nano-structures, *Phys. Stat. Sol. (b)* (2006) **243**: 1063-1079.

[28] Xu, Q., Sharma, A., Comer, B., Huang, H., Chow, E., Medford, A.J., Pask, J.E., and Suryanarayana, P., SPARC: Simulation Package for Ab-initio Real-space Calculations, *SoftwareX* (2021) **15**: 100709.

[29] Tsuchida, E., Choe, Y-K., and Ohkubo, T., An adaptive finite-element method for large-scale ab initio molecular dynamics simulations, *Phys. Chem. Chem. Phys.* (2015) **17**: 31444-31452.

[30] Pask, J.E. and Sterne, P.A., Finite element methods in *ab initio* electronic structure calculations, *Modelling Simul. Mater. Sci. Eng.* (2005) **13**: R71-R96.

[31] Motamarri, P., Das, S., Rudraraju, S., Ghosh, K., Davydov, D., and Gavini, V., DFT-FE - A massively parallel adaptive finite-element code for large-scale density functional theory calculations, *Comput. Phys. Commun.* (2020) **246**: 106853.

[32] Bowler, D.R., Choudhury, R., Gillan, M.J., and Miyazaki, T., Recent progress with large-scale ab initio calculations: the CONQUEST code, *Phys. Stat. Sol. (b)* (2006) **243**: 989-1000.

[33] Chelikowsky, J.R., Troullier, N., Wu, K., and Saad, Y., Higher-order finite-difference pseudopotential method: An application to diatomic molecules, *Phys. Rev. B* (1994) **50**: 11355-11364.

[34] Makov, G., Shah, R., Payne, M.C., Periodic boundary conditions in ab initio calculations. II. Brillouin-zone sampling for aperiodic systems, *Phys. Rev. B* (1996) **53**: 15513-15517.

[35] Corsetti, F. and Mostofi, A.A., System-size convergence of point defect properties: The case of the silicon vacancy, *Phys. Rev. B* (2011) **84**: 035209.

[36] Qian, X., Strahs, D., and Schlick, T., A new program for optimizing periodic boundary models of solvated biomolecules (PBCAID), *J. Comput. Chem.* (2001) **22**: 1843-1850.

[37] Mezei, M., Simulaid: A simulation facilitator and analysis program, *J. Comput. Chem.* (2010) **31**: 2658-2668.

[38] Wassenaar, T.A., de Vries, S., Bonvin, A.M.J.J., and Bekker, H., SQUEEZE-E: The Optimal Solution for Molecular Simulations with Periodic Boundary Conditions, *J. Chem. Theory Comput.* (2012) **8**: 3618-3627.

[39] Allen, M.P. and Tildesley, D.J., *Computer Simulation of Liquids*, Oxford University Press, Oxford, 1987.

[40] Massobrio, C., Du, J., Bernasconi, M., and Salmon, P.S. (Eds.), *Molecular Dynamics Simulations of Disordered Materials*, Springer, Switzerland, 2015.

[41] McConnell, K.J., Nirmala, R., Young, M.A., Ravishanker, G., and Beveridge, D.L., A Nanosecond Molecular Dynamics Trajectory for a B DNA Double Helix: Evidence for Substates, *J. Am. Chem. Soc.* (1994) **116**: 4461-4462.

[42] Schlick, T., Beard, D.A., Huang, J., Strahs, D.A., and Qian, X., Computational challenges in simulating large DNA over long times, *Comput. Sci. Eng.* (2000) **2**: 38-51.

[43] Briggs, E.L., Sullivan, D.J., and Bernholc, J., Real-space multigrid-based approach to large-scale electronic structure calculations, *Phys. Rev. B* (1996) **54**: 14362-14375.

[44] Natan, A., Benjamini, A., Naveh, D., Kronik, L., Tiago, M.L., Beckman, S.P., and Chelikowsky, J.R., Real-space pseudopotential method for first principles calculations of general periodic and partially periodic systems, *Phys. Rev. B* (2008) **78**: 075109.

[45] Sharma, A., Suryanarayana, P., On real-space Density Functional Theory for non-orthogonal crystal systems: Kronecker product formulation of the kinetic energy operator, *Chem. Phys. Lett.* (2018) **700**: 156-162.

[46] Dzwinel, W., Kitowski, J., and Mościński, J., ”Checker Board” Periodic Boundary Conditions in Molecular Dynamics Codes, *Mol. Sim.* (1991) **7**: 171-179.

[47] Bekker, H., Unification of box shapes in molecular simulations, *J. Comput. Chem.* (1997) **18**: 1930-1942.

[48] Cao, T., Ji, X., Wu, J., Zhang, S., and Yang, X., Correction of diffusion calculations when using two types of non-rectangular simulation boxes in molecular simulations, *J. Mol. Model.* (2019) **25**: 22.

[49] Hirose, K., Ono, T., Fujimoto, Y., and Tsukamoto, S., *First-Principles Calculations in Real-Space Formalism, Electronic Configurations and Transport Properties of Nanostructures*, Imperial Col-

lege Press, London, 2005.
[50] Tuckerman, M.E., *Statistical Mechanics: Theory and Molecular Simulation*, Oxford University Press, Oxford, 2010.